Geophysical Journal International

Geophys. J. Int. (2017) **208,** 1449–1464
Advance Access publication 2016 December 14
GJI Gravity, geodesy and tides

doi: 10.1093/gji/ggw467

GNSS related periodic signals in coordinate time-series from Precise Point Positioning

K.E. Abraha,[1] F.N. Teferle,[1] A. Hunegnaw[1] and R. Dach[2]

[1] *Institute of Geodesy and Geophysics, University of Luxembourg,* L-1359 *Luxembourg. E-mail: kibrom.abraha@uni.lu*
[2] *Astronomical Institute, University of Bern, Sidlerstrasse* 5, CH-3012 *Bern, Switzerland*

Accepted 2016 December 12. Received 2016 December 7; in original form 2016 July 15

SUMMARY

In Global Navigation Satellite System (GNSS) coordinate time-series unrecognized errors and unmodelled (periodic) effects may bias nonlinear motions induced by geophysical signals. Hence, understanding and mitigating these errors is vital to reducing biases and on revealing subtle geophysical signals. To assess the nature of periodic signals in coordinate time-series Precise Point Positioning (PPP) solutions for the period 2008–2015 are generated. The solutions consider Global Positioning System (GPS), GLObalnaya NAvigatsionnaya Sputnikovaya Sistema (GLONASS) or combined GPS+GLONASS (GNSS) observations. We assess the periodic signals of station coordinates computed using the combined International GNSS Service (IGS) and four of its Analysis Centers (ACs) products. Furthermore, we make use of different filtering methods to investigate the sources of the periodic signals. A faint fortnightly signal in our PPP solution based on Jet Propulsion Laboratory (JPL) products and the existence of an 8 d period for those ACs generating combined GPS+GLONASS products are the main features in the GPS-only solutions. The existence of the 8 d period in the GPS-only solution indicates that GPS orbits computed in a combined GNSS solution contain GLONASS-specific signals. The GLONASS-only solution shows highly elevated powers at the third draconitic harmonic (∼120 d period), at the 8 d period and its harmonics (4 d, 2.67 d) besides the well-known annual, semi-annual and other draconitic harmonics. We show that the GLONASS constellation gaps before December 2011 contribute to the power at some of the frequencies. However, the well-known fortnightly signal in GPS-only solutions is not discernible in the GLONASS-only solution. The combined GNSS solution contains periodic signals from both systems, with most of the powers being reduced when compared to the single-GNSS solutions. A 52 per cent reduction for the horizontal components and a 36 per cent reduction for the vertical component are achieved for the fortnightly signal from the GNSS solution compared to the GPS-only solution. Comparing the results of the employed filtering methods reveals that the source of most of the powers of draconitic and fortnightly signals are satellite-induced with a non-zero contribution of site-specific errors.

Key words: Time-series analysis; Satellite geodesy; Space geodetic surveys.

1 INTRODUCTION

Global Navigation Satellite System (GNSS) coordinate time-series (CTS) are known to be affected by unmodelled long-period signals and/or the propagation of sub-daily signals. These signals are caused by many factors. Satellite and receiver antenna modelling errors, mis-modelling of multipath signals, troposphere mis-modelling, solar radiation pressure (SRP) orbit modelling deficiencies and loading effects (atmosphere, ocean, hydrology) are some of the factors which may cause spurious signals in the CTS (Ge *et al.* 2005; Penna *et al.* 2007; Tregoning & Watson 2009; King & Watson 2010; Rodriguez-Solano *et al.* 2011; Griffiths & Ray 2012; Rodriguez-Solano *et al.* 2014; Santamaría-Gómez & Mémin 2015; Arnold *et al.* 2015; Sidorov & Teferle 2016). It is well established that one needs to have these effects in mind when using GNSS to study subtle geophysical signals and processes.

Global Positioning System (GPS) satellites have a revolution period of a half sidereal day and the constellation repeats once per sidereal day (GPS-ICD 1993; Agnew & Larson 2006). Hence the power spectrum of the GPS Position Dilution of Precision (PDOP) shows a prominent signal at one sidereal day (Dach *et al.* 2009) and sampling of the signal over a period slightly different from a sidereal day may introduce spurious signals. Ray *et al.* (2007) detected draconitic harmonics in the CTS of 167 International GNSS

source: https://doi.org/10.7892/boris.95200 | downloaded: 19.4.2024

© The Authors 2016. Published by Oxford University Press on behalf of The Royal Astronomical Society.

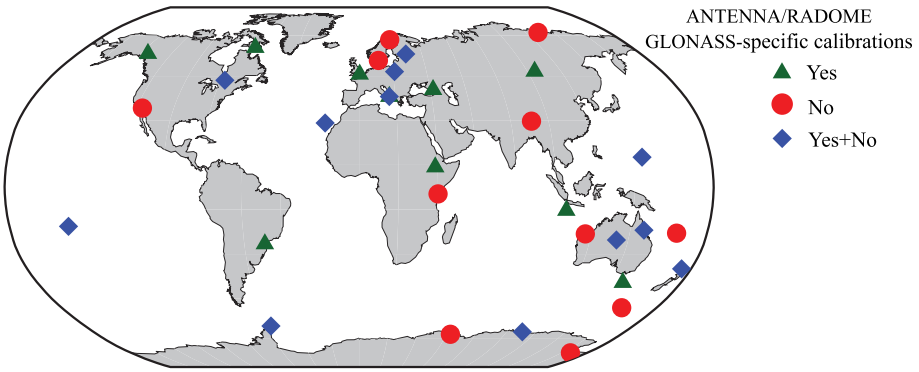

Figure 1. Selected GNSS stations from the IGS network, which are capable of observing both GPS and GLONASS used in this study. Symbols show the GLONASS-specific antenna/radome calibration for the period 2008–2015. Yes (green triangles) and No (red dots) indicate stations with and without GLONASS-specific antenna/radome calibration, respectively. Yes+No (blue diamonds) indicates stations where antenna/radome changes occur between 2008 and 2015 and hence have a combination of GLONASS-specific calibrated and uncalibrated antennas in the specified period. If GLONASS-specific calibrations are not available, the corresponding values from GPS-specific calibrations are assumed. All stations have GPS-specific antenna/none calibrations with few of them without antenna/radome calibrations. Though the antenna/radome combination information is provided here, the impacts of the GNSS-specific calibrations on the results are not studied in this paper.

Service (IGS; Dow *et al.* 2009) stations, which were part of the International Terrestrial Reference Frame 2005 (ITRF2005; Altamimi *et al.* 2007) network. The draconitic period is the time needed for the constellation to repeat its orientation to the Sun in an inertial frame. The time varies from one constellation to the other and it takes nearly 351.2 and 353.2 d to repeat the orientations for GPS and the Russian GLObalnaya NAvigatsionnaya Sputnikovaya Sistema (GLONASS), respectively.

Following Ray *et al.* (2007), several different studies have confirmed the existence of the draconitic harmonics in all GPS derived products (Amiri-Simkooei *et al.* 2007; Collilieux *et al.* 2007; Tregoning & Watson 2009; King & Watson 2010; Rodriguez-Solano *et al.* 2011; Griffiths & Ray 2012; Amiri-Simkooei 2013; Ray *et al.* 2013; Rodriguez-Solano *et al.* 2014; Arnold *et al.* 2015; Rebischung *et al.* 2015; Sidorov & Teferle 2016). Studies have indicated a high spatial correlation of the draconitic signals which indicates the major sources to be satellite-linked rather than site-specific (Collilieux *et al.* 2007; Ostini *et al.* 2007; Amiri-Simkooei 2013; Rebischung *et al.* 2015). Nevertheless, site-specific contributions to the powers of the draconitic frequencies have also been demonstrated (King & Watson 2010; Sidorov & Teferle 2016).

Subseasonal tidal signals, such as the fortnightly signal, are prominent periodic features which are known to exist in GPS CTS derived using products from the IGS or its analysis centres (ACs; Griffiths & Ray 2012; Ray *et al.* 2013). The tidal signal signature can have a direct and aliased nature due to parameter sampling (Griffiths & Ray 2012; Ray *et al.* 2013). A 13.63/13.66 d period from the direct and a 14.19/14.76 d period from the aliases are the largest tidal potential periods in GNSS CTS (Ray *et al.* 2013). For this study 13.6 d will be used to represent the direct (13.63/13.66 d) tidal periods. Another periodic feature which has been discovered since the inclusion of GLONASS observations to produce a combined GPS+GLONASS solution by some ACs is the periodic signal around 8 d (Meindl 2011; Ray *et al.* 2013; Arnold *et al.* 2015). This signal is related to the ground repeat period of the system (8 d). These GLONASS-specific signals are related to the system's satellites ground repeat period and they exists in all station coordinate components.

In this study, the nature of the periodic signals from different GNSS are assessed. We inspect the periodic signals in CTS from GPS-only, GLONASS-only and combined GPS+GLONASS Precise Point Positioning (PPP) solutions. Furthermore, we make use of an in-house produced double-differenced (DD) network solution using GPS-only observations. It should be noted that, hereafter, the term GNSS will be used to label the combined GPS + GLONASS solutions throughout the paper. The study briefly investigates the effects of model inconsistencies in a PPP processing strategy which is particularly relevant as we employ products computed from different GNSS software packages and we want to convince the reader of our high quality solutions. Moreover, the GPS-only and GLONASS-only solutions are assessed and compared to the GNSS solution over a selected global network of stations (Fig. 1). At last, to inspect the nature of the periodic signals, two different filtering methods are employed. We term the filtering methods as close-pair spatial-filtering and mask-filtering. The close-pair spatial-filtering follows the idea of the dual continuous GPS (dual-cGPS) station concept (Teferle *et al.* 2002) for which nearby stations are selected and coordinate differences are computed. For the mask-filtering, artificial observation masking, where a certain part of the horizon is masked, are simulated. The different features of the two filtering methods are compared and the possible sources of the periodic signals are discussed. The goal of the filtering methods is to filter out common signals and assess the possible sources of the periodic features.

The descriptions on the overall processing strategies are given in Section 2. Section 2 also demonstrates the influence of model inconsistencies in PPP. In Section 3, we compare and discuss the periodic nature of different solutions and filtering methods. Section 4 summarizes and concludes the main results.

2 GNSS PROCESSING STRATEGY

In this study we mostly used a PPP instead of a DD strategy. As PPP is based on a single station, the effects of site-specific errors such as multipath and certain obstructions can easily be assessed. Moreover, the computational efficiency and the independence of the network configuration makes PPP more attractive than DD for our purpose. Nevertheless, PPP can still deliver millimetre to decimetre levels of accuracy for both static and kinematic applications, respectively (Zumberge *et al.* 1997; Bisnath & Gao 2009; Geng

Table 1. Summary of processing settings.

Parameters	Description
GNSS software	Bernese GNSS Software version 5.2 (BSW52; Dach *et al.* 2015)
Strategy	Precise Point Positioning (PPP)
System(s)	GPS, GLONASS, GPS+GLONASS
Products	Satellite orbits & clocks and ERPs from: CODE, ESA, IGS, JPL, MIT
Signal	Ionospheric-free linear combination ($L3$)
Observable	Undifferenced, both code and phase. Code observations are down-weighted
Sampling rate	300 s
Elevation cut-off angle	3°
Observation weighting	Applied (elevation dependent weighting (w), $w = \cos^2 z$, with zenith angle z)
Ionospheric refraction	First order eliminated with $L3$, higher order modelled
Tropospheric refraction	*A priori* hydrostatic delay, 6-hourly European Centre for Medium-Range Weather Forecasts (ECMWF) Mapping Function, Vienna Mapping Function (VMF1, http://ggosatm.hg.tuwien.ac.at/DELAY) Troposphere parameters (every 2 hr) and north–south and east–west gradients (every 24 hr) are estimated with 5 m relative constraint
Ocean loading	Applied (FES2004 ocean tide model, http://holt.oso.chalmers.se/loading/)
Earth and polar tide	IERS2010 (Petit & Luzum 2010)
Antenna phase centre	igs08.atx file (http://igscb.jpl.nasa.gov/igscb/station/general/pcv_archive) Antenna phase centre offsets (PCOs) and phase centre variations (PCVs) corrected using GNSS-specific calibrations. - If no correction for antenna/radome* corresponding values are copied from antenna/none - If no GLONASS-specific antenna calibrations are available, values are adopted from GPS-specific calibrations. *see Fig. 1 for stations with and without GLONASS-specific antenna/radome calibrations
Estimated parameters	Station coordinates (daily), troposphere parameters (every 2 hr) and receiver clock corrections (epoch-wise)

et al. 2012) while mathematically the two processing strategies are equivalent (Dach *et al.* 2008). However, for comparison purposes DD results are also used and discussed. The PPP solutions are computed by fixing the final satellite orbits and clocks, and Earth Rotation Parameters (ERPs) in the Bernese GNSS Software version 5.2 (BSW52; Dach *et al.* 2015). In this study the employed products are from the IGS (Dow *et al.* 2009) and four IGS ACs, that is, the Center for Orbit Determination in Europe (CODE, ftp://ftp.igs.org/pub/center/analysis/code.acn), European Space Agency (ESA, ftp://ftp.igs.org/pub/center/analysis/esa.acn), Jet Propulsion Laboratory (JPL, ftp://ftp.igs.org/pub/center/analysis/jpl.acn) and Massachusetts Institute of Technology (MIT, ftp://ftp.igs.org/pub/center/analysis/mit.acn). The PPP processing details are described in Table 1.

With the advent of other GNSS, multi-GNSS PPP solutions have gained more attraction and focus of recent studies (Dach *et al.* 2009, 2010; Chen *et al.* 2013, 2015). The use of multiple GNSS provides improved satellite geometry and as a consequence improves position accuracies. Improvements have already been demonstrated for multi-GNSS combinations for high-rate and real-time applications (Wanninger & Wallstab-Freitag 2007; Ji *et al.* 2010) and for orbit estimation and long time-series effects (Dach *et al.* 2009; Meindl 2011; Fritsche *et al.* 2014; Arnold *et al.* 2015; Chen *et al.* 2015). However, in multi-GNSS data processing one has to give special attention to different biases which arise from the use of different systems and/or frequencies (Dach *et al.* 2010; Chen *et al.* 2013, 2015). These biases can be differential code biases (DCB) due to the hardware delay for Precise (P) and Coarse (C) codes, inter-frequency biases (IFB) due to the frequency dependency of different receivers and inter-systems biases (ISB)—a response of the receiver to different systems (Dach *et al.* 2015). In BSW52 the aforementioned biases are well handled and one bias (the sum of the three biases) can be estimated for code measurements. As the corresponding biases are absorbed by the ambiguity parameters they are not estimated for phase observations (Dach *et al.* 2015).

In GNSS data processing a reliable orbit model is vital because of the different satellite designs and characteristics of different systems. The Empirical CODE orbit model (ECOM, Beutler *et al.* 1994) which has been developed in the early 1990s was used by most of the IGS ACs until recently. However recent experiments, with the increased number of GLONASS satellites, indicated that the model has shortcomings for GLONASS and to improve the situation a new-ECOM has been developed by the CODE group (Arnold *et al.* 2015). With the release of this new-ECOM we updated our BSW52 orbit model to reduce the expected increase of RMS values during orbit fitting in case the old-ECOM is used to fit products produced using the new-ECOM. Nevertheless, we have made an experiment to test if there are any significant coordinate differences in our PPP solutions from fitting the products of the old-ECOM using the new-ECOM. This test was necessary as the operational CODE products have three phases (see ftp://ftp.unibe.ch/aiub/bswmail/bswmail.0335) and to demonstrate the influence of model inconsistencies in case of PPP (Teferle *et al.* 2007; Bock *et al.* 2012).

For CODE, the first phase products are produced before 2013 July 14 while the second phase products are produced between 2013 July 14 and 2015 January 4. The third phase products are produced from 2015 January 4 onwards. The main differences between the first and the second phase products are the no-SRP *a priori*

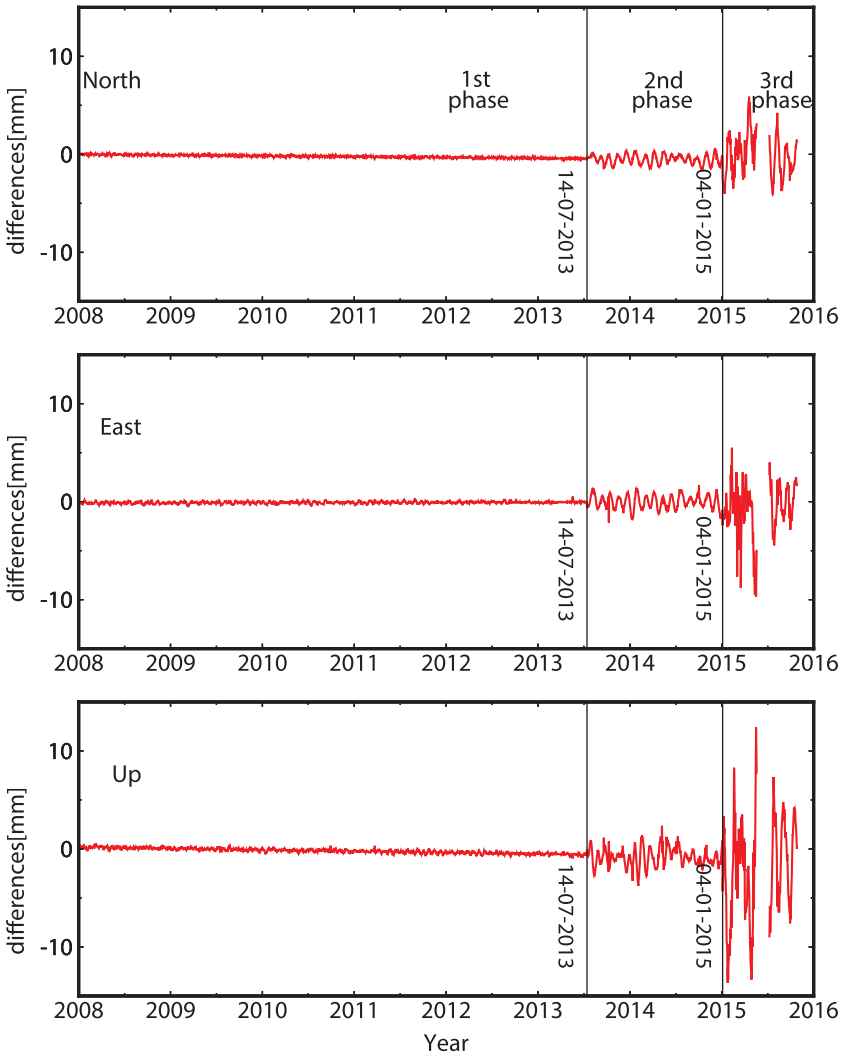

Figure 2. Coordinate differences for solutions estimated with an orbit fit of the old-ECOM and the new-ECOM for all components for station ONSA, Onsala, Sweden. GPS-only observations and CODE products were used. By orbit fitting we are referring to the polynomial representation of the inertial Cartesian positions of the satellites which is always the primary step while processing in BSW52. The upper, middle and lower panels are for north, east and up components, respectively. The vertical dark grey lines show the three phases of the CODE operational products (see the text for details).

model and applications of albedo and antenna thrust in the latter. In the first and second phases once-per revolution empirical SRP parameters are estimated. Besides a change in the angular argument, which is a minor issue regarding consistency, the main difference between the second and third phase products is that the twice and four-times per revolution SRP accelerations are estimated in the Sun direction in the latter phase (new-ECOM). Two PPP solutions are generated using IGS and the four ACs products for this specific experiment. In the first solution the orbits are fitted using the old-ECOM (where only once-per-revolution terms in all components and pulses at mid-night are set up) while in the second using the new-ECOM (the differences between the old and new ECOMs are described in Arnold *et al.* 2015). It should be mentioned that by orbit fitting we are referring to the polynomial representation of the inertial Cartesian positions of the satellites which is always the primary step in BSW52 GNSS data processing. The two solutions are created using the same settings as in Table 1 except for the polynomial representation of the orbits at the earliest stage of the processing and are labelled as old-ECOM and new-ECOM. Coordinate differences are computed between the two solutions for all products employed in this study and are compared with coordinates from ITRF2014 (http://itrf.ign.fr/ITRF_solutions/2014/) using the latter as a reference.

Fig. 2 shows the coordinate differences between the two solutions for station ONSA, Onsala, Sweden, for all coordinate components produced using GPS-only observations and CODE products. The dark grey vertical lines show epochs 2013 July 14 and 2015 January 4 to distinguish the periods of the different phases. Fig. 2 clearly shows that the new-ECOM represents well orbits, which are produced using the old-ECOM (first phase orbits) and the coordinate differences are negligible (∼0.1 mm for all components). However, for the second phase orbits the scatter of the coordinate differences of the two ECOMs reach 1 mm for the horizontal components and 3 mm for the vertical component. This is because of the fact that the albedo effect cannot be absorbed by the old-ECOM. Fitting the third phase orbits (orbits from the new-ECOM) with the old-ECOM might lead to coordinate differences of 5 mm for the horizontal and 10 mm for the vertical components. The reason here is that the albedo and the twice and four-times per revolution terms of the satellite accelerations cannot be absorbed by the old-ECOM. This

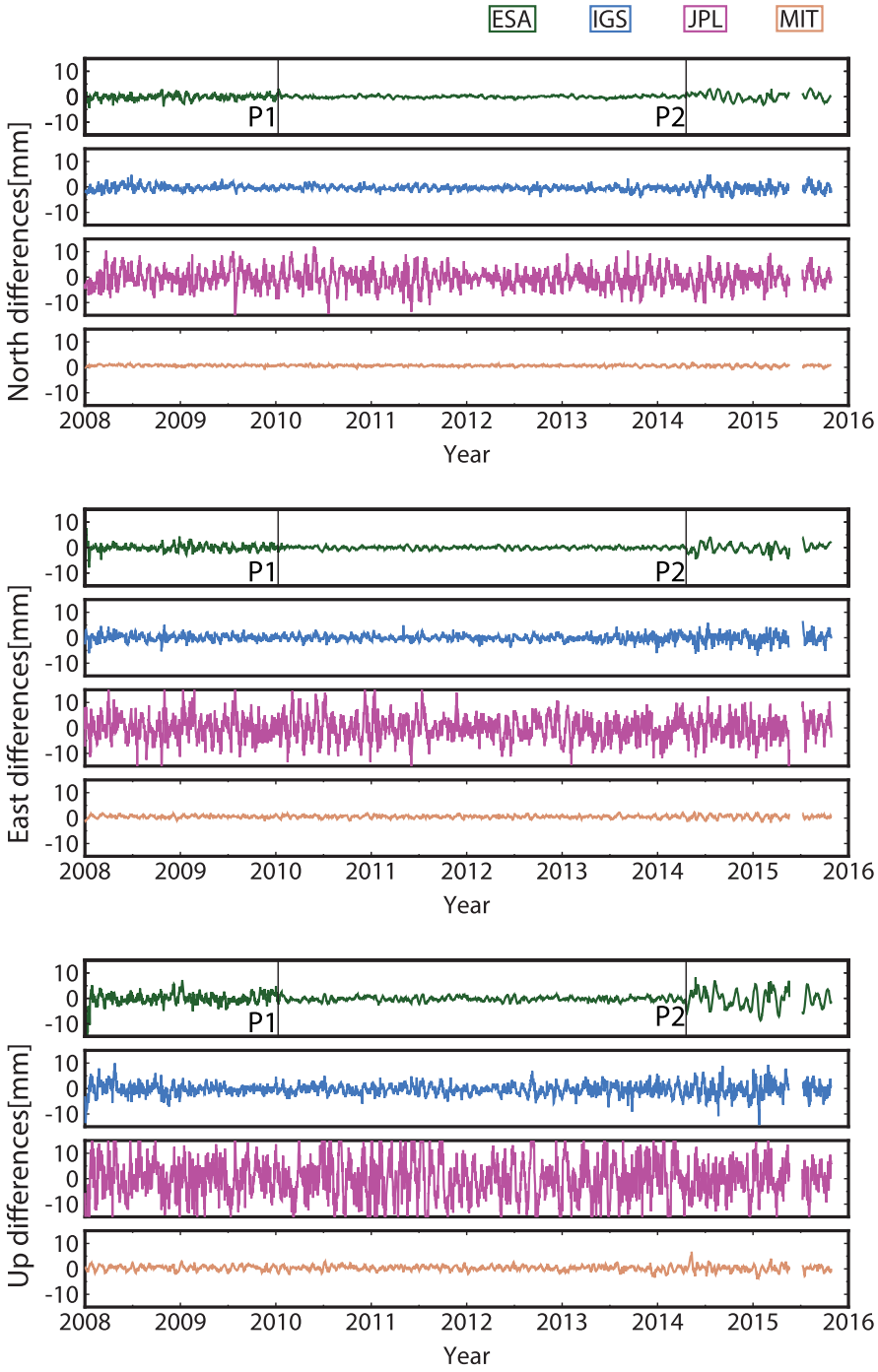

Figure 3. Coordinate differences between solutions estimated with an orbit fit of the old-ECOM and the new-ECOM for all components for station ONSA, Onsala, Sweden. The upper, middle and lower panels are for north, east and up components, respectively. The green, blue, magenta and brown colours (lines) are coordinate differences from a GPS-only solution with ESA, IGS, JPL and MIT products, respectively. P1 and P2 in the ESA solution panels show epochs 2010 January 10 and 2014 April 20, respectively, where major changes to the ESA orbit modelling were made (see the text for details).

shows that only the orbit model in the first phase is fully consistent with the product generation at CODE where the influence of the inconsistencies for the other phases can be seen from Fig. 2. For the combined IGS and other ACs products (Fig. 3) similar effects of inconsistencies can be expected as it is not possible to achieve full consistency as in the first phase of the CODE products.

Fig. 3 shows the coordinate differences between the two solutions produced using GPS-only observations and IGS, ESA, JPL and MIT products for the same station (ONSA, Onsala, Sweden). Four different behaviours can be observed in Fig. 3 for the coordinate differences created using the four different products. The differences for ESA (green lines in Fig. 3) show different characteristics before P1, between P1 & P2 and after P2 (see vertical grey lines and P1 & P2 texts in Fig. 3). The vertical grey lines (P1 & P2) in the ESA based solution in Fig. 3 indicate the periods January 10, 2010 and April 20, 2014, respectively. The ESA products become more consistent to the different orbit models in the periods between P1 and P2 where the differences are more scattered before and after

Table 2. Coordinate differences between the ITRF2014 and the solutions in Section 2. The coordinate differences are computed between solutions based on PPP by fitting (polynomial representation of) the orbits using the new-ECOM & old-ECOM and the ITRF2014 solution for station ONSA, Onsala Sweden (see the text). The ITRF2014 coordinates of the station are used as a reference and the mean and RMS of coordinate differences are computed accordingly for the two solutions using products from CODE, ESA, IGS, JPL and MIT. The table the shows mean and RMS of the differences for north (N), east (E) and up (U) components in mm.

	Mean of coordinate differences						RMS of coordinate differences					
	new-ECOM			old-ECOM			new-ECOM			old-ECOM		
Product	N	E	U	N	E	U	N	E	U	N	E	U
CODE	0.00	0.05	0.09	−0.08	0.07	−0.14	1.80	2.35	4.03	1.85	2.37	4.07
ESA	0.06	−0.03	0.08	0.07	−0.04	0.08	2.44	3.50	4.32	2.51	3.53	4.55
IGS	−0.06	0.04	0.29	−0.10	0.01	0.16	2.71	4.58	6.02	2.85	4.74	6.26
JPL	−0.05	0.17	0.13	−0.11	0.11	−0.08	3.43	5.66	8.10	4.77	7.08	11.19
MIT	−0.04	0.01	0.04	−0.05	0.00	−0.09	1.43	2.20	3.99	1.42	2.19	3.90

P1 and P2, respectively. For the period before P1 it can be related, among other unknown reasons which are out of the scope of this study to identify, to the software modifications they have made. ESA started to produce products using a modified software since GPS week 1566 (2010 January 10) as indicated in the IGS mail (https://igscb.jpl.nasa.gov/pipermail/igsmail/2010/006133.html) which is the period where the scatter starts to be (highly) reduced in Fig. 3. The higher scatter after P2 is due to the major change in the ESA orbit modelling where they started to use a box-wing model (Rodriguez-Solano *et al.* 2012) as an *a priori* for SRP since GPS week 1789 (2014 April 20).

The coordinate differences are more stable over time for the JPL (magenta lines) and MIT (brown lines) products in Fig. 3. However, the coordinate differences (scatter) are higher for JPL compared to all products used here. This can be related to the different stochastic filters in their orbit modelling compared to all other ACs. The coordinate differences from MIT are less scattered compared to all ACs (but more scattered than CODE for the first phase orbits). This shows that the MIT products are produced using the old-ECOM for the whole period used in this study and are well represented using the new-ECOM. For the coordinate differences created using the IGS products (blue lines in) higher scatter can be seen starting from 2014 compared to the period before 2014. This can be related to the ESA and CODE solutions dominating the IGS combination. Overall, the coordinate differences are less scattered for the IGS products. In the combined IGS products the effects of the model changes are less pronounced. However, the consistency of the PPP processing is not on the same level as for any of the individual AC solutions which is the reason for the higher scatter for IGS compared to the ACs such as CODE, ESA and MIT (Fig. 3). For all products, the repeatability of the coordinates are improved when the orbits are represented using the new-ECOM.

Both old-ECOM and new-ECOM solutions are compared with the coordinates from the ITRF2014 to see how much our PPP solutions are away. Comparing the solutions with the ITRF2014 coordinates (see Table 2), for station ONSA, the RMS of the (Up) coordinate differences ranges between 4 and 8 mm with the mean of the differences nearly zero for all products. The agreement between the solutions with the ITRF2014 coordinates is 3–5 per cent better for the new-ECOM compared to the old-ECOM. In general, the coordinate differences are at a comparable level for both old-ECOM & new-ECOM and for all products except for JPL where the scatter (RMS) of differences is higher. The main point of this experiment is to show the sensitivity of the PPP strategy to products and orbit modelling consistencies. In case of a full consistency (e.g. first phase in Fig. 2) a PPP strategy can achieve the full accuracy potential as a network DD solution. Modelling discrepancies cause uncertainties and reflect in the resulting CTS (Figs 2 and 3). For consistency the results of this study, which are presented in the next sections, are all based on parameters estimated with orbit fitting using the new-ECOM and hence the consistency is guaranteed. It should be noted that the results of this section do not show which products are better but highlight the consistency of the products with the orbit model in BSW52 and the sensitivity of PPP strategy for model inconsistencies.

3 RESULTS

GPS-only, GLONASS-only and GNSS PPP solutions are generated using IGS, CODE, ESA, JPL and MIT products from a selected global set of GNSS stations (Fig. 1). The GPS-only solutions are produced from IGS and all the aforementioned ACs while the GLONASS-only and GNSS solutions are produced using ESA products only. To investigate the different periodic features in our PPP CTS we have computed stacked power spectra over all stations for all solution types. In addition to that, the same spectra are produced for coordinate differences caused by simulated artificial masking (mask-filtering) and coordinate differences between nearby stations (close-pair spatial-filtering). The latter is essentially the same as the procedure applied for the dual-cGPS stations as have been investigated in Teferle *et al.* (2002). This section covers the solutions in different subsections.

3.1 GPS-only solutions

To gain more insight into our CTS, we have plotted the normalized power spectra of PPP-based, de-trended CTS computed using GPS-only observations and products from CODE, ESA, IGS, JPL and MIT for the period 2008-2015. The power spectra are stacked for all stations and then smoothed with a boxcar smoother (e.g. Ray *et al.* 2007). The consistency of the solutions was guaranteed as has been outlined above which means that the differences between the solutions are solely due to the products. Fig. 4 shows the result of the stacked power spectra plotted with frequencies (cycles per year (cpy)) in the x-axis and normalized power in the y-axis for all components for the GPS-only solutions. The dark grey vertical lines show the annual and semi-annual signals, the light grey dashed lines show the cycles per draconitic year (cpdy; 1cpdy = 1.04 cpy) up to the 10th harmonics, 13.6 d (fortnightly, ∼14 d) period and ∼8 d period.

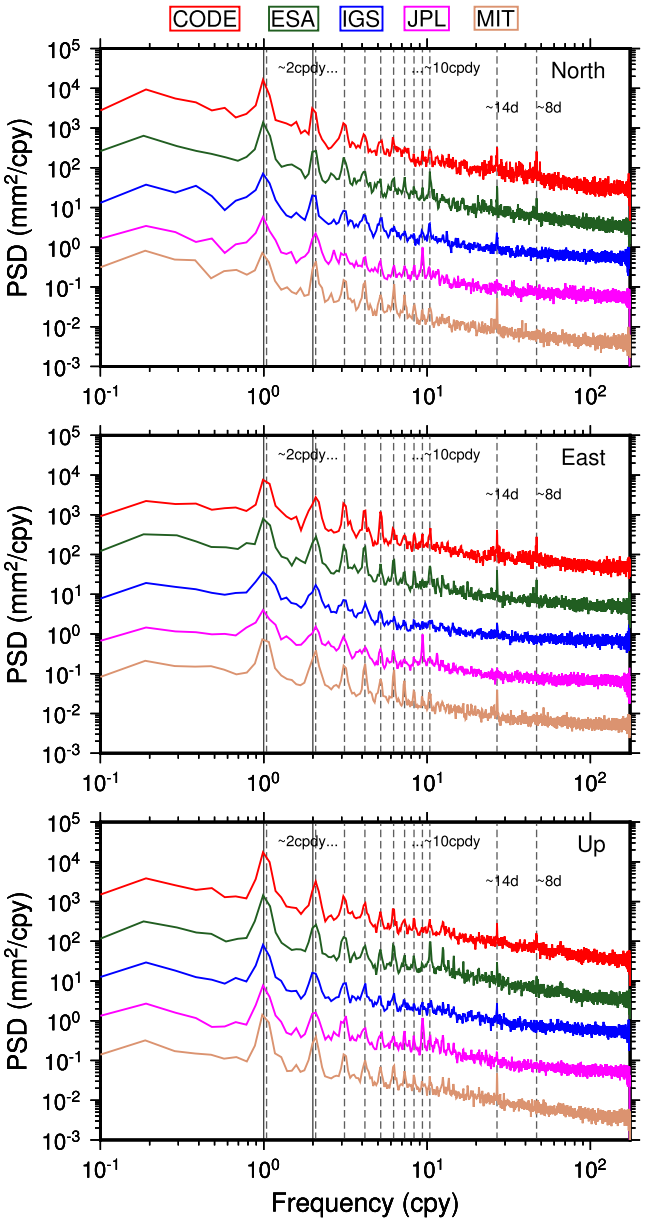

Figure 4. Power spectra of CTS (stacked from all stations in Fig. 1) for GPS-only solutions using the CODE, ESA, IGS, JPL and MIT products. The power spectra of the solutions have been shifted along the vertical axis for clarity. The dark grey vertical lines are the annual and semi-annual cycles, the light grey dashed lines are the 1.04 cpy and its harmonics (until the 10th harmonic), the fortnightly 14 and 8 d period cycle.

At first glance the general features of the power spectra of our PPP CTS are identical to the features seen in global solutions of other studies (Ray *et al.* 2007; Rebischung *et al.* 2015, 2016). As PPP uses satellite orbits and clocks created in a global network solution, the two pictures (the PPP and global solutions) are expected to be identical. This confirms that our PPP solutions are correctly and properly created. Besides, two remarkable points can be highlighted in Fig. 4. The first is the faint fortnightly signal (the 13.6 d period) in all components computed using the JPL products compared to the others. The faint fortnightly signal in JPL is also confirmed by Rebischung *et al.* (2015) from their analysis of the second IGS reprocessing campaign (repro2) ACs CTS.

The very existence of the signal in the PPP solutions produced using all ACs and the IGS products may indicate it is a signal coming from an error in the International Earth Rotation and Reference Systems Service (IERS) tide models (e.g. for solid Earth tidal variations in the geopotential). However, the reason for the smaller signal in our PPP solution using JPL products is not clear but might be attributed to the stochastic character of their filter. Assuming that the unmodelled geopotential acceleration is absorbed by the stochastic characteristic of their (JPL) orbit model, one might expect the existence of the signal in a PPP solution produced using their products. However, only a faint nature of the signal is shown in Fig. 4. Furthermore, the signal is less pronounced in the horizontal components compared to the vertical component.

The second and most interesting signal is the existence of the 8 d period in the power spectra of CTS computed using both CODE and ESA products but not from those of IGS, JPL and MIT. The 8 d period is a well-known signal and has been associated with the repetition rate of the GLONASS constellation with respect to the ground network. However, it should be noted that the PPP solutions in Fig. 4 are computed using GPS-only observations and products. Only the GPS orbits have been extracted from the multi-GNSS products of CODE and ESA for this PPP solution. This is an indication that the GPS-only orbits, which are computed in a rigorous way from the combined GPS and GLONASS data processing, contain a GLONASS-specific signal. Studies in the past described that the combination of GPS and GLONASS neither improves nor degrades the GPS-only orbit precision (Fritsche *et al.* 2014). On the other hand, Dach *et al.* (2012) have shown that enabling the GLONASS ambiguity resolution had also a positive impact on the GPS orbits. However, it is clear that the GPS products from GNSS ACs (specifically CODE and ESA as in this study) carry a GLONASS-specific period. The signal is more powerful in the horizontal components (specially in the East component) than in the vertical component. Nevertheless, the stacked spectra reduces significantly the noise floor and that this signal would have a reduced impact in any CTS.

The following points can be used to argue that the signal is an effect of GLONASS over the GPS. First, the signal does not exist in the PPP solutions based on the IGS and other ACs products. Second, to our knowledge, there is no known periodic feature at this frequency other than the GLONASS-specific signal in the GNSS solutions. To understand the nature of the signal in a global network solution we selected global stations which are used by CODE in their repro2 solution. The British Isles continuous GNSS Facility (BIGF) and University of Luxembourg Tide Gauge Benchmark Monitoring (TIGA; Schöne *et al.* 2009) analysis centres (BLT) have completed a global GPS-only solution as a contribution to the IGS TIGA working group using latest models and IERS conventions. The solution is completed employing data of more than 700 stations using a network DD strategy in BSW52 where ambiguities are resolved in baselines of up to 6000 km. The global solution is created by extracting and fixing GPS-only orbits from CODE repro2 products (Steigenberger *et al.* 2014) for the period before 2013 December 28 and CODE operational final products (Dach *et al.* 2016) for the period between 2013 December 29 and 2015 December 31. The details of the processing strategy can be seen in Hunegnaw *et al.* (2016). A total of 161 global stations, which are also used by CODE in their repro2 and daily routine processing, were selected from the 700+ stations. The stacked power spectra of the de-trended, de-seasoned CTS are computed and plotted in Fig. 5 using the same 161 stations for five different time windows. The time windows where the power spectra are computed are

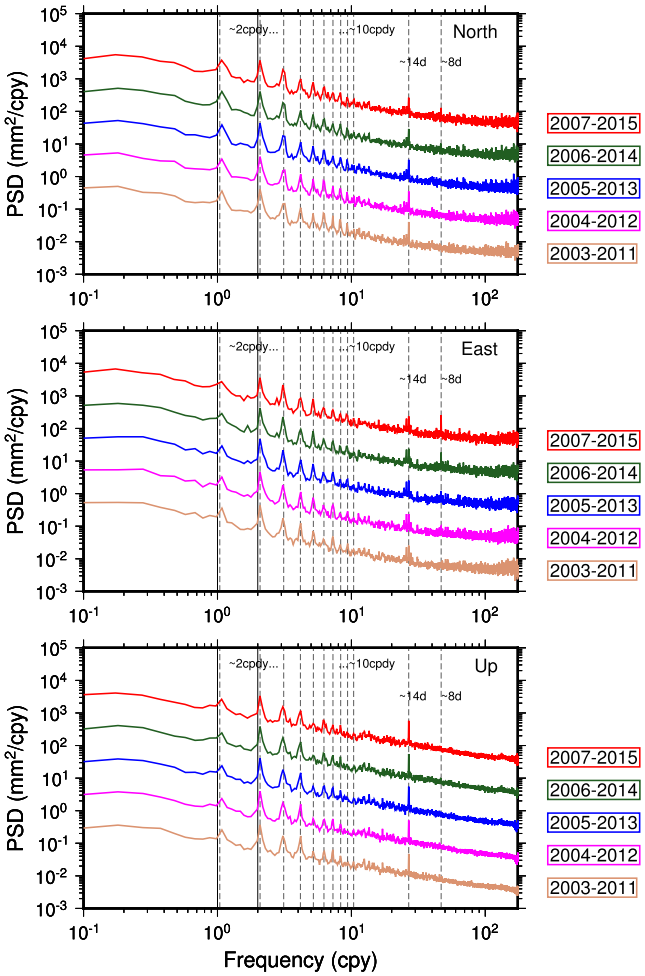

Figure 5. Power spectra of de-trended and de-seasoned CTS stacked from 161 global set of stations from the BLT repro2 solution. The solution was computed in a double-differenced network strategy using GPS-only observations and CODE products. The spectra are computed and stacked for the same stations but for different time windows (2003–2011, 2004–2012, 2005–2013, 2006–2014, 2007–2015—see colour codes). The power spectra of the different windows have been shifted along the vertical axis for clarity. The vertical lines are as described in Fig. 4.

2003–2011, 2004–2012, 2005–2013, 2006–2014, 2007–2015. All defined time windows have the same length (9 yr) in order to have similar resolution of the frequencies. The reason we started in 2003 is that CODE started to include GLONASS observations in their solution since then.

Fig. 5 shows that the draconitic signals and the fortnightly period have very similar features for the windows. However, there is a clear variation in the 8 d period for the different time windows. The 8 d period in a global GPS-only solution is faint in the Up component while it is powerful in the East component. The signal is faint in all components for the windows 2003–2011, 2004–2012 but it starts to show up in the horizontal components for the windows 2005–2013, 2006–2014 and 2007–2015, where it becomes very clear especially in the East component for the latter two windows. This is an indication that GLONASS observations start to contribute more to the solution since the system regained its full constellation in December 2011. Moreover, the number of GLONASS tracking stations increases starting from 2007 (see fig. 2 in Fritsche *et al.* 2014) and so is the contribution of GLONASS to the global solution.

The striking nature of the 8 d period in the East component can be related to unsuccessful ambiguity resolution. Compared to the PPP solutions, the period has less power (faint for the Up component) in the global network solution, which indicates that a certain part of the signal is reduced by differencing and ambiguity resolution. In the GPS constellation, the main change in the aforementioned windows is a modernization of the system where 11 BLOCK IIF satellites were included in the constellation at the end of 2015 (3, 4, 8 and 11 BLOCK IIF satellites were available in 2012, 2013, 2014 and 2015, respectively).[1] Accordingly, one might suspect that the BLOCK IIF satellites could contribute to the signal. However, as the fortnightly and draconitic periods are more consistent in time, and the 8 d period doesn't exist in the solutions using products from IGS and other ACs, we hypothesize that the 8 d period in the GPS-only solutions is clearly a GLONASS effect. However, for a detailed understanding on how a GLONASS-specific 8 d period shows up in a GPS-only solution one will need a global solution with orbits and other parameters estimated and this is beyond the scope of the study.

3.2 GLONASS-only solutions

Stacked power spectra of the CTS produced from GLONASS-only observations are computed for the same stations as shown in Fig. 1 for the period 2009–2015. Only ESA products are used to produce the solutions as the IGS and other ACs do not provide GLONASS satellite clock products over the time span. Fig. 6 (upper panel) shows the result of the stacked power spectra of the CTS plotted against frequencies (cpy) in the *x*-axis and normalized power in the y-axis. The dark grey vertical lines show the annual and semi-annual signals, the light grey dashed lines show cycles per draconitic year (cpdy; 1cpdy = 1.034cpy) up to the 10th harmonic, the 13.6 d (fortnightly, ∼14 d) period, and the ∼8 d period and its second and third harmonics. It should be noted that 1.034 cpy instead of 1.04 cpy is used as the draconitic year for GLONASS is different, that is, 353.2 d.

As with the GPS-only solutions, the draconitic signal peaks are visible to the 9th and 10th harmonic in the stacked power spectra of the GLONASS-only CTS (Fig. 6, upper panel). The very striking features in the GLONASS-only solution are the elevated power of the third draconitic harmonic and the 8 d period and its harmonics. The third harmonic is very pronounced and is the nearly 120 d signal discovered by Meindl (2011). This signal is nearly one-third of a year and the elevated power is related to the three orbital planes of the GLONASS system.

The other striking features in the GLONASS-only CTS are the 8 d period and its harmonics (second and third). The clear visibility of the associated second (peaks at 4.03, 3.99 and 3.94 d) and third (peaks at 2.67 and 2.63 d) harmonics of the 8 d period (peaks at 8.2, 7.98 and 7.8 d) is a clear indication that they are caused by systematic errors in the orbits which reappear due to the ground repeat of the constellation. These harmonics, however, are faint in the stacked power spectra of GNSS ACs CTS in their repro2 solutions (Rebischung *et al.* 2015). This can be explained by the fact that their solutions are from the processing of combined observations. In addition, the reason for the faint second and third harmonics of the 8 d period in the GNSS ACs repro2 solutions can be related to the domination of the GPS-only tracking network and observations.

[1] http://www.navcen.uscg.gov/?Do=constellationstatus

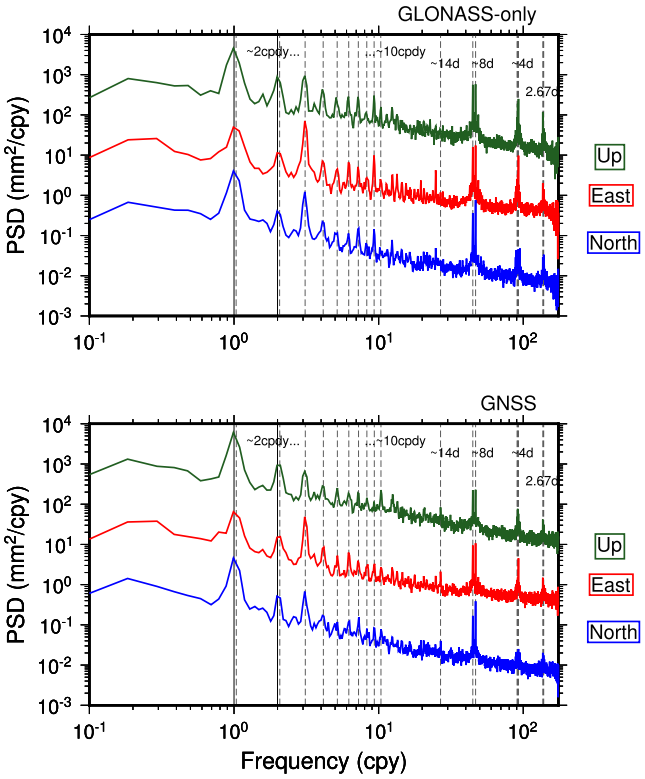

Figure 6. Power spectra of CTS (stacked from all stations in Fig. 1) for GLONASS-only (upper panel) and GNSS (lower panel) solutions using ESA products. In both panels the power spectra of the components have been shifted along the vertical axis for clarity. For the upper panel the dark grey vertical lines are the annual and semi-annual cycles, the light grey dashed lines are the 1.034 cpy and its harmonics (until the 10th harmonic), the fortnightly and 8 d period and its harmonics (4 and 2.67 d). For the lower panel a mean value of 1.037 cpy is adopted as the solution contains signals from both systems and the vertical grey lines indicate the harmonics up to degree 10. The other dashed lines are as in the upper panel.

The GLONASS constellation was incomplete before December 2011. We suspect that the gaps in the constellation might have been contributing to the spectrum at some of the frequencies. To investigate this contribution to the spectrum, we make a comparison by creating solutions before and after the completion of the constellation. This comparison might not be fully optimal as the stations have different data gaps, GLONASS-specific antenna/radome calibrations (see Fig. 1) and the satellite orbit and clock products might have different quality (e.g. Figs 2 and 3) before and after December 2011. To avoid this effect, we have made a GLONASS-only PPP solution for the period 2012-2015, where GLONASS was complete (reference solution). In addition, we created two more GLONASS-only PPP solutions for the same period but by excluding satellites which have not been part of the constellation before 2012 (see Fig. 7). Taking the solution with 24 satellites as the reference solution, solutions two and three are created using 16 and 20 satellites, respectively. Solution two is to assume the constellation gap in the period 2008–2010 while solution three is to assume the gap in the period 2010–2011.

Comparing the three solutions shows that the gaps in the constellation contribute to the spectrum of some of the frequencies (Fig. 8). The affected periods are the ∼8 d period and its harmonics and the ∼120 d period. The gaps in the constellation largely affect the ∼4 and ∼2.67 d periods compared to the main ∼8 d period. From the 8 d period, the ∼7.8 d period is more consistent for the three

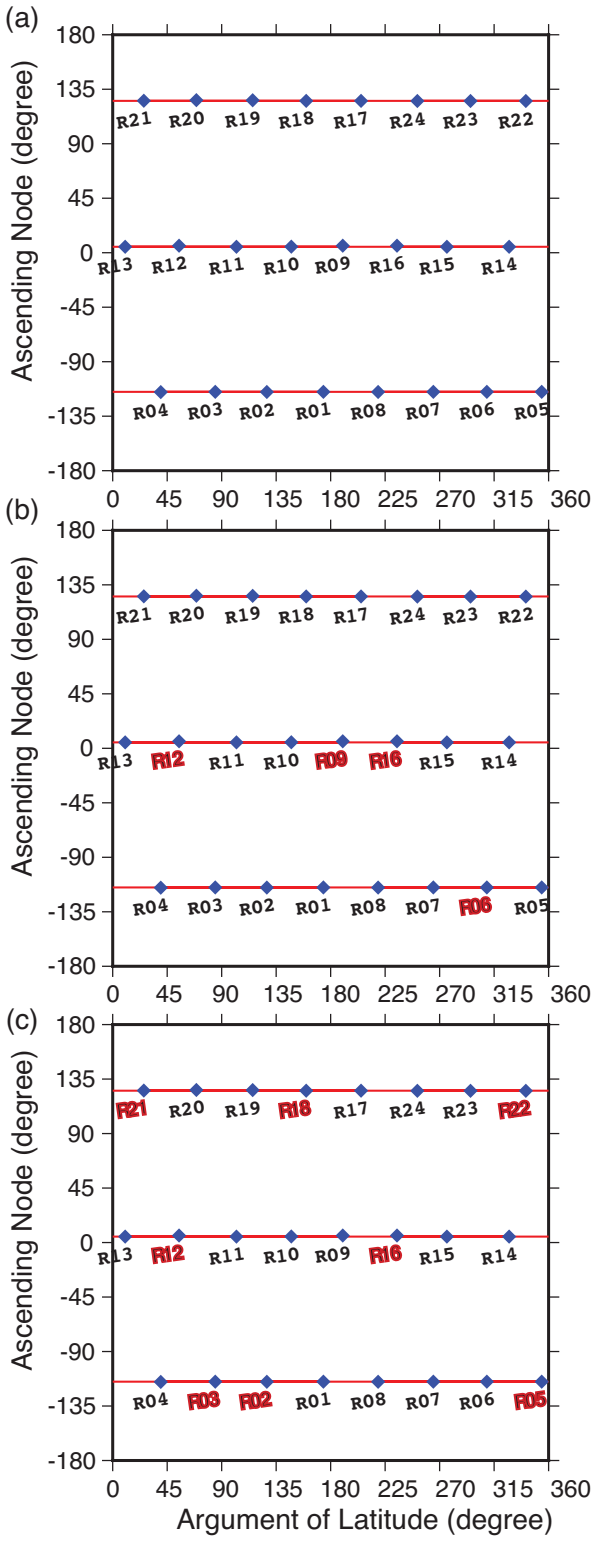

Figure 7. Ascending node Vs argument of latitude of GLONASS constellation as of 2012 July 18. (a) the complete constellation with 24 GLONASS-M (blue diamonds) satellites which is used to create the reference solution. (b) 20 GLONASS-M satellites used for the second solution where satellites with red text are excluded from contributing to the solution. (c) 16 GLONASS-M satellites used for the third solution where satellites with red text are excluded from contributing to the solution. The three solutions are created with the same modelling and processing settings except for the excluded satellites in each solution.

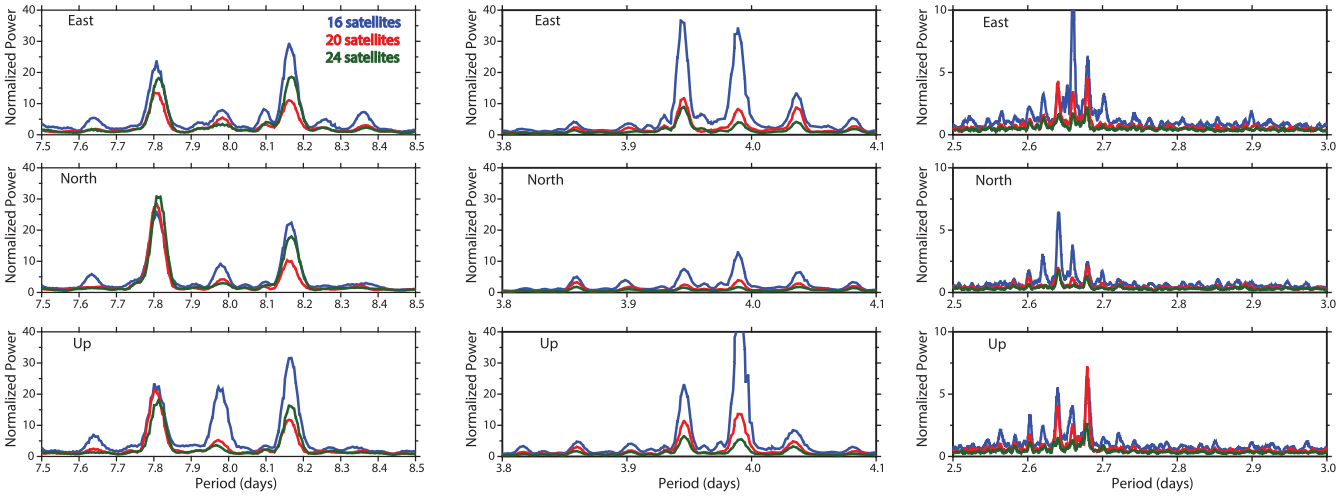

Figure 8. High frequency section of power spectra of CTS (stacked from all stations in Fig. 1) for the three GLONASS-only PPP solutions using 16 (blue), 20 (red) and 24 (green) satellites (see Fig. 7). The three solutions are computed using ESA products. The power spectra of the three solutions are normalized to the same scale. The left, middle and right panels are for 8, 4 and 2.67 d periods, respectively. The X-axis shows the period in days.

different solutions, while the ∼7.98 d and ∼8.2 d periods are more affected by the constellation gaps. This can be seen from Fig. 8 where the powers are similar for the solutions with 16, 20 and 24 satellites for the 7.8 d period. This 7.8 d is the pervasive GLONASS-specific 8 d period as seen already in Figs 4 and 5, and also in the repro2 solutions of the GNSS ACs (Rebischung *et al.* 2015, 2016). The gaps played a role in the ∼4 d (4.03, 3.99 and 3.94 d) period where the reference solution has nearly no power at the specified frequencies compared to the other two solutions. The same holds for the third harmonic of the 8 d period (∼2.67 d) where again the powers are faint for the solution with 24 satellites compared to solutions with 16 and 20 satellites. The gaps also contribute to the nearly third draconitic harmonic (∼120 d signal). Comparing solutions with 24 and 16 satellites, a ∼23 per cent power reduction of the ∼120 d period is achieved by the former (figure not shown here), but the power starts to be consistent for the solutions with 24 and 20 satellites.

Another feature from the GLONASS-only solution is the non-existence of the main fortnightly signal. Fig. 6 (upper panel) shows that the main fortnightly signal at the 13.6 d period (direct tide), which is expected to be caused by the error in the tidal models, is not identifiable in the power spectra of the CTS. Since GLONASS and GPS orbits are estimated using the same software and orbit model, the non-existence of the fortnightly signal in the GLONASS-only solution can be a surprise. The fortnightly signal is present in all GPS-only solutions using products from the IGS and all ACs. Assuming that the signal is a tidal phenomenon one expects the signal to also be present in both GPS-only and GLONASS-only solutions. The signal is quite consistent in the GPS-only solution for the different time windows (Fig. 5). This suggests that the different satellite blocks (the GPS constellation modernization) do not affect the solutions in different manners. In the case of GLONASS, the non-existence of the fortnightly signal is consistent throughout, that is, no effect is seen from the constellation gaps experiment.

We have two hypothesis on this issue. First, the non-existence of the fortnightly signal in the GLONASS-only solution, if the signal comes from an error in the IERS tidal models for the solid Earth tidal variations in the geopotential, can be related to a shallow resonance of GLONASS satellites with the Earth rotation. GPS satellites are in a deep 2:1 resonance with the Earth orbit (16 revolutions per 8 sidereal days) while GLONASS satellites are in shallow resonance (17 revolutions per 8 sidereal days) (Dach *et al.* 2009). Second, the signal could be an unmodelled orbit effect which is then finally mapped into CTS where in this case, it is completely absorbed by the orbit parameters in the GLONASS-only solution. However, more experiments are needed to get a detailed understanding of this issue and this is beyond the scope of this study. Nevertheless, this shows that the fortnightly signal is more sensitive to the orbit dynamics of the GNSS, while GPS is more affected due to the deep resonance with the Earth rotation and tidal processes close to (semi-) diurnal periods compared to GLONASS.

A significant signal at 14.76 d period is evident in the GLONASS-only solution. The signal is more pronounced for the horizontal (mainly East) components while it has a faint nature in the Up component. This period is an alias effect of the errors in the tides due to the 24 hr data processing scheme (Ray *et al.* 2013). This signal has a faint nature in our GPS-only results (Fig. 4).

3.3 GNSS (GPS + GLONASS) solutions

Stacked power spectra of CTS from a combined GNSS solution is computed for the same stations as shown in Fig. 1. As our data length (7 yr) does not allow to resolve the two draconitic periods of the systems (351.2 for GPS and 353.2 for GLONASS), we adopt a mean draconitic period of 352.2 d and its harmonics (vertical grey lines in the lower panel of Fig. 6) as in Fritsche *et al.* (2014). As one would expect, the stacked power spectra of the CTS from the GNSS solution contains signals from both systems (lower panel of Fig. 6). However, it is worth noting that most of the system-specific periods mentioned in Sections 3.1 and 3.2 are highly reduced for the combined solution (Table 3). This is a clear indication of the benefits of such a combined solution. In general, Table 3 shows the power reduction over draconitic, fortnightly and 8 d periods of GNSS solution compared to GPS-only and GLONASS-only solutions. In the table positive values show a reduction and negative values show an enhancement of power.

The main GPS-only signals which are reduced due to adding GLONASS to the solution are the draconitic harmonics and the fortnightly signal. The reduction of the fortnightly signal is very

Table 3. Power reduction (in per cent) over draconitic, fortnightly and 7.8 d period signals of GNSS solution compared to GPS-only and GLONASS-only solutions using ESA products. The length of the GPS-only solution is reduced to the same period as the GLONASS-only solution for consistency. To avoid the impact of the GLONASS constellation gap on the powers of some of the frequencies, the power comparisons are made for the period 2012 onwards. Positive values show a power reduction while negative values show a power enhancement.

	Power reduction (per cent)					
	GPS			GLONASS		
Period	North	East	Up	North	East	Up
1 cpdy	− 29.0	37.9	1.2	20.8	0.7	7.0
2 cpdy	23.8	60.5	21.1	15.8	16.1	35.4
3 cpdy	− 51.5	− 128.8	− 8.8	63.3	48.5	59.3
4 cpdy	12.4	58.8	6.6	39.1	15.9	58.0
5 cpdy	12.7	29.8	7.3	29.2	30.0	49.1
6 cpdy	13.9	42.0	44.0	22.6	52.7	63.2
7 cpdy	− 11.3	31.5	3.98	31.7	63.8	63.0
8 cpdy	11.2	29.8	27.4	8.5	46.3	2.73
13.6 d	52.0	52.2	36.7			
7.8 d				23.5	31.7	55.9

striking and reaches 52 per cent for the horizontal components and 36 per cent for the vertical component (Table 3). This can explain why the power spectra of the repro2 CTS from CODE have very small amplitude in the 13.6 d period, especially in the Up component. The little power in the 13.6 d period is true for all GNSS ACs in their repro2 CTS as can be seen in Rebischung *et al.* (2015) but the reduction is striking for CODE and the reason could be the inclusion of GLONASS in CODE's processing since 2002 (ESA includes GLONASS only since 2009).

However, there are some frequencies where the power gets enhanced by including GLONASS to the GPS-only solution. The effect is more obvious for the third draconitic harmonics (∼120 d period). In general, the inclusion of GLONASS benefits more the horizontal components of the GNSS solution than the vertical component. The power reduction of GPS-only periods due to adding GLONASS is more significant in the even draconitic harmonics than the odd ones. The more pronounced power reduction for the even harmonics in the GNSS solution is a clear GLONASS effect. Very strong odd draconitic harmonics for GLONASS have been shown by Meindl (2011) for the geocentre Z-component. The existence of the 8 d period and its harmonics in the GNSS solution (lower panel of Fig. 6) is also another clear effect of including GLONASS in the solution. Table 3 also shows that GLONASS benefits more from the GNSS solution for all draconitic harmonics compared to GPS. The reason is attributed to the fact that the number of GPS observations dominates those of GLONASS for all stations. For GLONASS-only solution the vertical component benefits more compared to the horizontal components and the power reduction reaches 60 per cent in some of the draconitic harmonics.

A direct comparison of the powers for the GPS-only and GLONASS-only solutions shows that nearly all frequencies have (very) enlarged power for the latter (results not shown here). However, we argue that this is not optimal comparison as the former dominates in terms of antenna/radome calibration (see Fig. 1), orbit and clock quality, global network coverage and number of observations. We would expect the effect of GLONASS to be more significant once it reaches at a comparable level to GPS in terms of the aforementioned factors.

3.4 Discussion

As the existence of the aforementioned periodic signals in CTS has been confirmed, the main question remains on the source and possible ways of mitigating them. With the main driver of the energy being debated its sources can be classified into ground and space-based. The ground-based sources are due to local (site-specific) effects at stations. This happens as satellite-station geometry repeats at a certain period for a given GNSS (one sidereal day for GPS, 8 sidereal days for GLONASS) and a parameter sampling causes an aliasing of periods. The space-based sources can be classified into a geometrical (number of planes, satellite inclination, repetition rates, eclipsing periods etc.) and on orbit modelling parts (SRP modelling remains a dominant component). Another factor could be the aliasing effects of the Earth Orientation Parameters (EOP) tidal errors which resonate with the GNSS orbital periods.

Previous studies demonstrated a spatial correlation of the draconitic signals and their inspection indicated that the main contribution of the draconitic powers are satellite-linked (Amiri-Simkooei 2013; Rebischung *et al.* 2015). Nevertheless, site-specific linkage to the powers have also been demonstrated (King & Watson 2010; Sidorov & Teferle 2016). To clarify the sources of the periodic signals, two filtering methods are proposed here. The first filter is a masking-filter, which is performed by simulating an obstruction mask in a certain part of the horizon thereby ignoring the observations in that direction. Then the coordinate differences for the same station with and without the mask are computed. The second filter is a close-pair spatial-filtering, which is performed by computing coordinate differences between two nearby stations. Teferle *et al.* (2002) termed this a dual-cGPS station pair and applied the method to CTS of cGPS stations with short observation time spans.

For the mask-filtering approach an artificial masking scenario is simulated using an azimuth dependent masking feature in our modified version of BSW52 (Abraha *et al.* 2016). For this section two different PPP solutions are created. One (the reference solution) using the existing data as in the above sections while the second solution is by implementing the artificial mask as in Fig. 9(a). Both solutions follow the same settings, procedure (Table 1), models and products except for the implemented mask and hence the consistency of the solutions is guaranteed. It is worth mentioning here that the features seen from the mask-filtering are observed from any kind of mask (different scenarios in the north, east, west and other directions are tested, results not shown) irrespective of its severity and azimuthal direction and coverage.

Fig. 9 shows the sky plot of GPS (blue lines) and GLONASS (red lines) satellites before (panel b) and after (panel c) the mask (panel a) is considered. The simulated mask is implemented for all stations in the network to produce the second solution. The differences between the coordinates of the two solutions are computed and we termed this as mask-filtering. As we have ensured a fully consistent processing of the observations with and without masking, the differences in the coordinates can be solely attributed to the assumed mask. This is performed for GPS-only and GNSS solutions and the stacked power spectra of the coordinate differences for both solutions are computed.

Fig. 10 shows the percentage of missing data (left panel) due to the obstruction mask and its power spectra (right panel) for station ONSA, Onsala, Sweden. One can see considerably system-specific features in the figure. The main features are powers at a sidereal day for GPS and 1/3 of a sidereal day for GLONASS which are linked

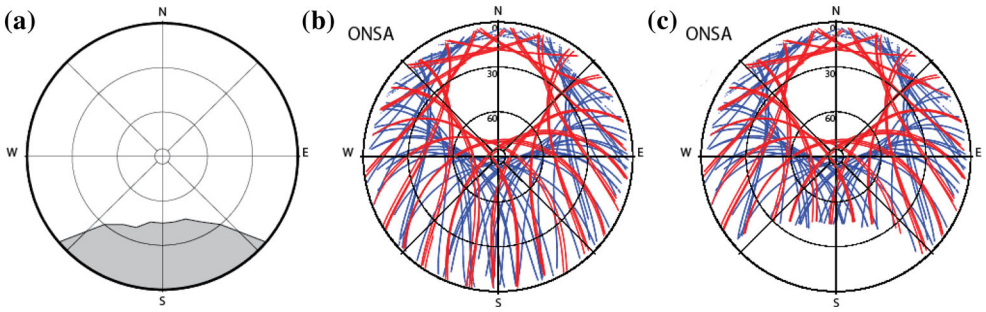

Figure 9. (a) Obstruction mask simulated in the south direction between azimuths 130° and 230° (grey colour is the masked part of the sky); (b) the actual skyplot for station ONSA, Onsala, Sweden, without mask; (c) the skyplot with the mask in (a) applied. In panels (b) and (c), the blue and red lines denote the sky-tracks for GPS and GLONASS satellites, respectively.

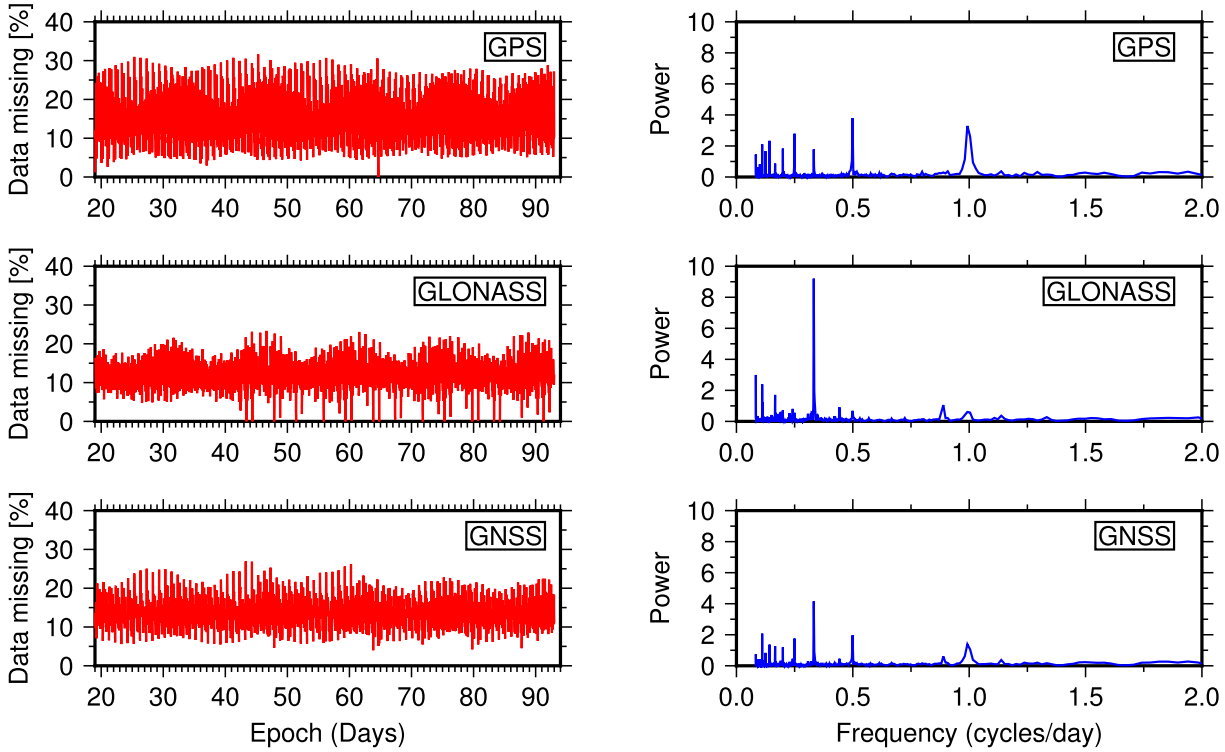

Figure 10. Percentage of missing data (left panel) and associated power spectra (right panel) for station ONSA, Onsala, Sweden. Red line is the hourly time-series of percentage of missing data caused by the mask as in Fig. 9, blue line is the power spectra of the percentage of missing data time-series. Upper, middle and bottom panels are for GPS-only, GLONASS-only and GNSS, respectively.

to the geometry repeat of the satellites (Dach *et al.* 2009). Of course the GNSS solution contains all signals from both systems but with reduced power. These features can be an indication that obstructions (or anything which changes the geometry) can cause errors which may propagate into long-term CTS with GNSS-specific periods as was described in Abraha *et al.* (2016). Similar features are observed for all stations (results not shown).

In general, for most of the stations the percentages of missing data range between 10 per cent and 22 per cent. The implemented mask is in a certain direction and hence the amount and quality of data masked may vary from station to station as systematic errors like multipath are site-specific. Hence, the masking may reduce systematically noisy data (e.g. due to multipath) for some stations while for others the results are degraded as the good data is masked.

Figs 11 and 12 show the stacked power spectra of the coordinate differences due to the simulated mask as shown in Fig. 9 for GPS-only and GNSS solutions, respectively. The mask-filtering is performed for every station in the network and the power spectra of the coordinate differences are stacked together. The main results of Figs 11 and 12 can be described as follows; clear draconitic signals up to the 10th harmonic, the sudden flattening of the power spectra, clear visibility of the fortnightly signal and the disappearance of the 8 d period in the differences for the GPS-only solution which was observed in Figs 4 and 5. We return to the aforementioned features shortly. For a better explanation of those features a set of nearby stations are selected from the IGS network (Fig. 13). The dual-cGPS stations in Fig. 13 all have baseline distance of less than 10 km. A GPS-only PPP solution using CODE products is created with the same strategy as in Section 3.1 for the stations in Fig. 13. Finally coordinate differences are computed between the dual-cGPS stations (close-pair spatial-filtering) and stacked power spectra are computed.

Essentially the close-pair spatial-filtering removes the satellite effects and eliminates common signals (King & Williams 2009)

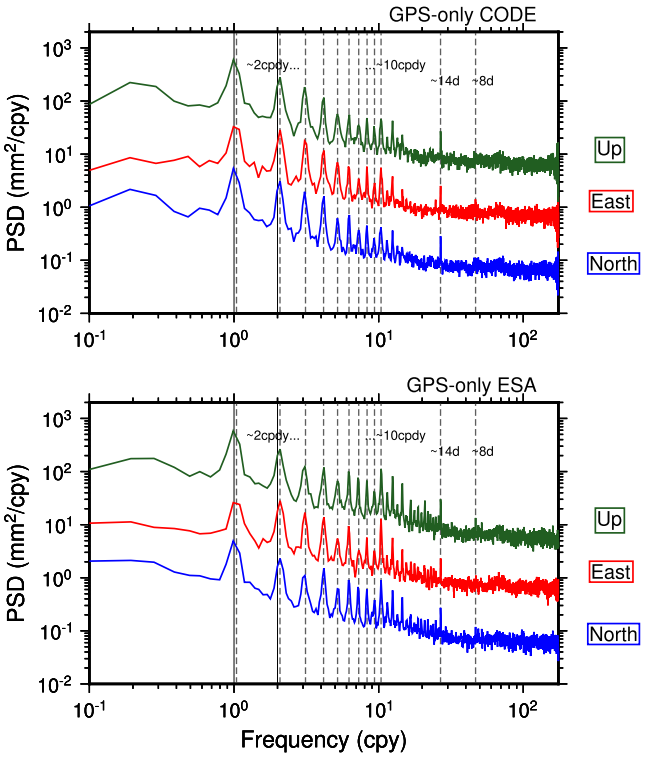

Figure 11. Power spectra of the coordinate differences due to the mask in Fig. 9 (stacked from all stations in Fig. 1) for the GPS-only solution using the CODE (upper panel) and ESA (lower panel) products. The power spectra of the components have been shifted along the vertical axis for clarity. The vertical lines are as described in Fig. 4.

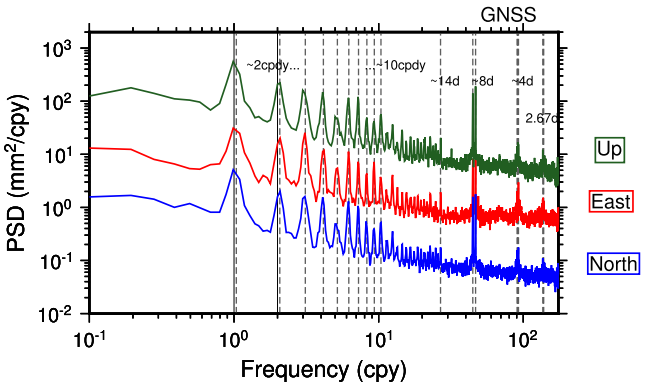

Figure 12. Power spectra of coordinate differences due to the mask in Fig. 9 (stacked from all stations in Fig. 1) for the GNSS solution using ESA products. The power spectra of the components have been shifted along the vertical axis for clarity. The vertical lines are as described in the lower panel of Fig. 6.

as nearby stations observe similar satellite geometry. The stacked power spectra of this filter (Fig. 14) shows most of the higher order draconitic signals are substantially reduced with some remaining small powers. These remaining powers are an indication that local effects such as multipath and receiver antenna calibration errors are still contributing to the draconitic signals supporting the findings of King & Watson (2010) and Sidorov & Teferle (2016). The close-pair spatial-filtering also removes the fortnightly signal (but exists prominently in the mask-filtering, see next paragraph) which is an indication that the major effect of the 13.6 d period also originates at the satellite level. Moreover, the fortnightly signal would

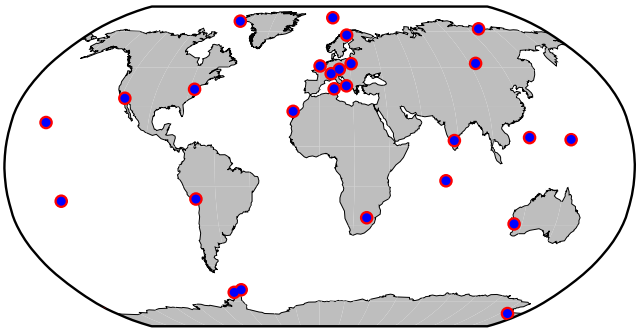

Figure 13. Site locations which are selected for the close-pair spatial filtering (blue-red pair on the map). The maximum baseline used for the close-pair spatial-filtering is 10 km.

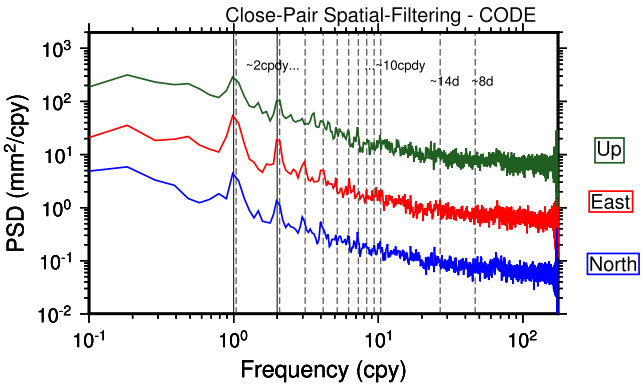

Figure 14. Power spectra of the close-pair spatial-filtering computed and stacked for 26 baselines as shown in Fig. 13. The power spectra of the components have been shifted along the vertical axis for clarity. The vertical lines are as described in Fig. 4. CODE GPS-only products were used to generate the results.

also be removed if the tide model contained similar error for the nearby stations, as one would expect.

However, unlike close-pair spatial-filtering, the mask-filtering shows a very prominent power at the draconitic and fortnightly periods. Simulating a mask for a certain station means taking out a certain amount of observations (Fig. 10) and hence changing the satellite geometry as seen by a specific station. Basically, the coordinate differences between solutions with and without the obstruction (mask-filtering) for the same station can be equivalent to computing coordinate differences between two stations which observe different satellite characteristics (satellite geometry, multipath environment, observation rate etc.). Consequently, the stacked power spectra of the coordinate differences contain elevated powers for periods of the draconitic and fortnightly signals. This shows that most of the draconitic powers are originating at the satellite level and is in agreement with previous studies, which have demonstrated a high spatial correlation of the draconitic signals (Amiri-Simkooei 2013; Rebischung *et al.* 2015). This holds true also for the fortnightly signal as its existence is prominent in the mask-filtering in contrast to the close-pair spatial-filtering.

Another interesting feature from both filtering methods is the elimination of the GLONASS-only signal in the GPS-only solutions. This can be an indication that the GLONASS-only signal contained by the GPS orbits might be the same for all satellites but this remains to be confirmed. This is in agreement with the results in Fig. 5, which suggests that a certain amount of the signal is reduced during differencing. Fig. 12 shows stacked power spectra of

the coordinate differences due to the mask from a GNSS solution. The same features as in Fig. 11 can be seen from the mask-filtering of the GNSS solution. Moreover, highly elevated powers at the 8 d period and its harmonics are visible. This is again an indication that the 8 d period and its harmonics are caused by the ground repeat of the constellation with the constellation gap contributing to some extent.

Finally, the last feature in the stacked power spectra of the coordinate differences of the mask-filtering is the sudden change in the nature of the noise (Figs 11 and 12). Normally, the stacked power spectra of the CTS (Figs 4 and 6) closely follow a coloured and white noise process with the latter being clear at the highest frequencies. However, the power spectra of the mask-filtering clearly shows a higher flattening level (a clear change of coloured to white noise) near 7–8 d. This is an indication that more white noise is added due to the mask. A detailed noise analysis would confirm this but is deemed beyond the scope of the study.

4 SUMMARY AND CONCLUSION

In GNSS CTS nonlinear motions triggered by geophysical signals may be biased by some technical errors and unmodelled effects. A good understanding of the errors and possible mitigation mechanisms are vital when using the time-series to study subtle geophysical processes. The annual and semi-annual signals are the two most well-known prominent signals in GNSS CTS where nearly 40 per cent of the powers are caused by geophysical fluid mass loads redistribution (Dong *et al.* 2002). Since Ray *et al.* (2007), other prominent signals which are harmonics of the GNSS draconitic year (351.2 d for GPS, 353.2 d for GLONASS) have become well known periodic features. In addition, the fortnightly signal has been a well-known periodic feature. Previous studies indicated that most of the signals are satellite-linked with some part of them to be contributed by site-specific errors such as multipath. One example can be errors in the EOP which are known to be absorbed into the orbit estimates which eventually result in draconitic and fortnightly signals. With the advent of GLONASS and some IGS ACs including its observations in their routine processing, GLONASS-specific periods (elevated power of the third draconitic harmonics, 8 d period) have also been discovered (Meindl 2011).

Our PPP based stacked power spectra of CTS estimated using GPS-only, GLONASS-only and combined GPS+GLONASS products of the IGS and its individual ACs (CODE, ESA, MIT and JPL) show prominent signals at the annual, semi-annual, draconitic and its harmonics as well as fortnightly and 8 d periods. The annual, semi-annual, and draconitic signals are clear in all solutions computed using the aforementioned products and the general picture of the power spectra is similar to the global solution reported by previous studies.

The fortnightly signal (13.6 d period) exists in all GPS-only solutions with the solution based on JPL products showing a very faint nature for this signal. The faint nature of the signal was also reported in JPL's repro2 solution. However, one might expect the existence of the signal in a PPP solution based on their products, which is shown here that the signal is soaked. Though the existence of the signal in all our GPS-only PPP solutions based on the IGS and other ACs products might indicate a relation to an error in the IERS tide models, the faint nature of the signal in the JPL based solution remains unexplained. One might claim that the signal is absorbed by the stochastic character of their processing filter as their orbit modelling is different from other ACs. However, the GLONASS-only solution does not show any feature at the fortnightly period. This is a rather unexpected result as the GPS+GLONASS products are estimated with the same software and orbit models. The GLONASS products used here are from ESA which are produced based on a rigorous GPS+GLONASS combined solution. Extracting GPS-only and GLONASS-only orbits from this combined product and producing PPP solutions using the observations and orbits from one system show a prominent 13.6 d period for the GPS-only solution while it is not visible in the GLONASS-only solution. This raises a question whether this signal is a tidal phenomenon or an unmodelled orbit error which then maps into the coordinates. In the latter case, it could be an unmodelled orbit issue which is then fully absorbed by the products during their generation. If it was a tidal phenomenon, one expects the signal to appear in both systems. However, the reason might be linked to the deep resonance of GPS orbit repeats with the Earth rotation and tidal errors close to (semi-) diurnal periods which makes it to be more affected by the tidal effects than GLONASS. This needs a further detailed analysis which is beyond the scope of this study.

The GLONASS-only solution shows very clear features at a nearly 8 d period and its harmonics. The 8 d period has second and third harmonics which indicates that the period is related to systematic errors in the satellite orbits which reappear as the ground geometry repeats. The 8 d period has features at 8.2, 7.98 and 7.8 d, its second harmonic at 4.03, 3.99 and 3.94 d, and the third harmonic at 2.67 and 2.63 d. From the 8 d period, the nearly 7.8 d period signal is consistent in power while the others are affected by the gaps in the GLONASS constellation. The gaps in the constellation highly contribute to the second and third harmonics of the 8 d period as well. The elevated power at the third harmonic of the draconitic period from the stacked power spectra of the GLONASS-only solution is another very prominent signal. This signal is the nearly 120 d period and confirms the findings of Meindl (2011). The gaps in the constellation also found to be contributing to some extent to this period. The 8 d period which is now known as a GLONASS-specific period exists also in the GPS-only PPP solutions produced using CODE and ESA products. This is a rather unusual signal as the solutions are computed using GPS-only products which indicates that the GPS-only orbits contain a GLONASS-specific feature. It is shown that certain amount of the power of the 8 d period in the GPS-only solution is reduced by differencing and the existence of the signal is more prominent in recent time windows (2013–2015), which shows that GLONASS starts to contribute more to the global solution.

System-specific signals are largely reduced in the combined GPS+GLONASS solution. The GLONASS-only solution benefits more from the combined solution compared to the GPS-only solution with the power reduction reaching 60 per cent in some of the frequencies. A significant reduction is observed from the GPS+GLONASS solution for the fortnightly signal compared to the GPS-only solution. The reduction reaches 52 per cent for the horizontal components and 36 per cent for the vertical component (Table 3). The system-specific signals arise from systematic errors of a specific GNSS which recur due to different orbital plane structures, orbit repeatability and incomplete constellation. Similar effects can be expected from the other new GNSS such as the European Galileo and Chinese BeiDou system (BDS). For Galileo and BDS the orbit repeatabilities are 10 and 7 d, respectively. Periodic signals associated with the orbital repeat frequencies can be expected in CTS derived using these systems and more reduction of system-specific signals can be achieved combining all systems.

Using the azimuth-dependent masking feature in BSW52 artificial observation masks were simulated and used as a mask-filtering method. The stacked power spectra of the coordinate differences caused by the simulated masks (mask-filtering) show very clear peaks at the draconitic periods extending to the 10th harmonic and a very clear fortnightly signal. For comparison, coordinate differences are computed between nearby stations and the stacked power spectra of the coordinate differences (close-pair spatial-filtering) show that most of the draconitic signals and the fortnightly period disappear. Comparing the mask-filtering and close-pair spatial-filtering, with the former showing very prominent and the latter faint draconitic and fortnightly signals, indicates that the major sources of the power of the signals are satellite-linked rather than site-specific. However, some remaining power in the latter filter still indicates a contribution to the draconitic harmonic signals from site-specific errors such as multipath and receiver antenna modelling errors. The 8 d period noticed in the GPS-only solution disappeared from both filters which is an indication that it is to some extent a uniform effect for all satellites which can be reduced by differencing.

ACKNOWLEDGEMENTS

KEA is funded by the Fonds National de la Recherche Luxembourg (contract number 6835562) and AH is funded by the University of Luxembourg internal research projects GSCG and SGSL. The computational resources used in this study were provided by the High Performance Computing Facility at the University of Luxembourg (ULHPC). We also acknowledge Jim Ray for his valuable discussions and the IGS, CODE, ESA, JPL and MIT for data and products. The constructive comments of Alvaro Santamaría-Gómez, Junping Chen, an anonymous reviewer, and editor Kosuke Heki are highly appreciated.

REFERENCES

Abraha, K.E., Teferle, F.N., Hunegnaw, A. & Dach, R., 2016. Impact of limited satellite visibility on estimates of vertical land movements, *Int. Assoc. Geodesy Symposia,* doi:10.1007/1345_2016_231.

Agnew, D.C. & Larson, K.M., 2006. Finding the repeat times of the GPS constellation, *GPS Sols.,* **11**(1), 71–76.

Altamimi, Z., Collilieux, X., Legrand, J., Garayt, B. & Boucher, C., 2007. ITRF2005: a new release of the International Terrestrial Reference Frame based on time series of station positions and Earth Orientation Parameters, *J. geophys. Res.,* **112,** B09401, doi:10.1029/2007JB004949.

Amiri-Simkooei, A.R., 2013. On the nature of GPS draconitic year periodic pattern in multivariate position time series, *J. geophys. Res.,* **118**(5), 2500–2511.

Amiri-Simkooei, A.R., Tiberius, C.C.J.M. & Teunissen, P.J.G., 2007. Assessment of noise in GPS coordinate time series: methodology and results, *J. geophys. Res.,* **112**, B07413, doi:10.1029/2006JB004913.

Arnold, D. *et al.*, 2015. CODE's new solar radiation pressure model for GNSS orbit determination, *J. Geod.,* **89**(8), 775–791.

Beutler, G., Brockmann, E., Gurtner, W., Hugentobler, U., Mervart, L., Rothacher, M. & Verdun, A., 1994. Extended orbit modeling techniques at the CODE processing centre of the International GPS Service for geodynamics (IGS): theory and initial results, *Manuscr. Geod.,* **19**(6), 367–384.

Bisnath, S. & Gao, Y., 2009. Current state of precise point positioning and future prospects and limitations, in *Observing our Changing Earth, Int. Assoc. Geodesy Symposia*, vol. 133, pp. 615–623, ed. Sideris, M.G., Springer.

Bock, H., Dach, R. & Jäggi, A., 2012. Impact of inconsistent use of IERS Conventions on PPP results, Presented at European Geosciences Union General Assembly, 2012 April 22–27, Vienna, Austria.

Chen, J., Pei, X., Zhang, Y. & Wu, B., 2013. GPS/GLONASS system bias estimation and application in GPS/GLONASS combined positioning, in *Lecture Notes in Electrical Engineering,* vol. 244, pp. 323–333, *China Satellite Navigation Conference (CSNC) 2013 Proceedings*, eds Sun, J., Jiao, W., Wu, H. & Shi, C., Springer.

Chen, J., Zhang, Y., Wang, J., Yang, S., Dong, D., Wang, J., Qu, W. & Wu, B., 2015. A simplified and unified model of multi-GNSS precise point positioning, *Adv. Space Res.,* **55**(1), 125–134.

Collilieux, X., Altamimi, Z., Coulot, D., Ray, J. & Sillard, P., 2007. Comparison of very long baseline interferometry, GPS, and satellite laser ranging height residuals from ITRF2005 using spectral and correlation methods, *J. geophys. Res.,* **112,** B12403, doi:10.1029/2007JB004933.

Dach, R., Beutler, G. & Gudmundsson, G.H., 2008. Analysis of GPS Data from an Antarctic Ice Stream, in *Observing our Changing Earth, Int. Assoc. Geodesy Symposia,* vol. 133, pp. 569–579, ed. Sideris, M.G., Springer.

Dach, R. *et al.*, 2009. GNSS processing at CODE: status report, *J. Geod.,* **83**(3–4), 353–365.

Dach, R., Schaer, S., Lutz, S., Meindl, M. & Beutler, G., 2010. Combining the observations from different GNSS, in *EUREF 2010 Symposium,* 2010 June 2–5, Gävle, Sweden.

Dach, R. *et al.*, 2012. Annual Center Reports: Center for Orbit Determination in Europe (CODE), in *International GNSS Service, Technical Report 2011,* pp. 29–40, eds Meindl, M., Dach, R. & Jean, Y., IGS Central Bureau.

Dach, R., Lutz, S., Walser, P. & Fridez, P.E., 2015. *Bernese GNSS Software Version 5.2. User Manual,* Astronomical Institute, Universtiy of Bern, Bern Open Publishing.

Dach, R., Schaer, S., Arnold, D., Orliac, E., Prange, L., Susnik, A., Villiger, A. & Jäggi, A., 2016. *CODE Final Product Series for the IGS,* Published by Astronomical Institute, University of Bern, URL: http://www.aiub.unibe.ch/download/CODE.

Dong, D., Fang, P., Bock, Y., Cheng, M. & Miyazaki, S., 2002. Anatomy of apparent seasonal variations from GPS-derived site position time series, *J. geophys. Res.,* **107,** B42075, doi:10.1029/2001JB000573.

Dow, J.M., Neilan, R.E. & Rizos, C., 2009. The International GNSS Service in a changing landscape of Global Navigation Satellite Systems, *J. Geod.,* **83**(3–4), 191–198.

Fritsche, M. *et al.*, 2014. Homogeneous reprocessing of GPS, GLONASS and SLR observations, *J. Geod.,* **88**(7), 625–642.

Ge, M., Gendt, G., Dick, G., Zhang, F. & Reigber, C., 2005. Impact of GPS satellite antenna offsets on scale changes in global network solutions, *Geophys. Res. Lett.,* **32,** L06310, doi:10.1029/2004GL022224.

Geng, J., Williams, S.D.P., Teferle, F. & Dodson, A.H., 2012. Detecting storm surge loading deformations around the southern North Sea using subdaily GPS, *Geophys. J. Int.,* **191**(2), 569–578.

GPS-ICD, 1993. *GPS Interface Control Document, Revision C (ICD-GPS-200C)*. US Departement of Defense (DoD), URL: http://www.navcen.uscg.gov/pubs/gps/icd200/.

Griffiths, J. & Ray, J., 2012. Sub-daily alias and draconitic errors in the IGS orbits, *GPS Solut.,* **17**(3), 413–422.

Hunegnaw, A., Teferle, F.N., Bingley, R.M. & Hansen, D.N., 2016. Status of TIGA Activities at the British Isles Continuous GNSS Facility and the University of Luxembourg, in *IAG 150 Years: Proceedings of the IAG Scientific Assembly*, Postdam, Germany, 2013, vol. 143, pp. 617–623, eds Rizos, C. & Willis, P., Springer.

Ji, S., Chen, W., Ding, X., Chen, Y., Zhao, C. & Hu, C., 2010. Potential benefits of GPS/GLONASS/GALILEO integration in an Urban Canyon – Hong Kong, *J. Navig.,* **63**(04), 681–693.

King, M.A. & Watson, C.S., 2010. Long GPS coordinate time series: multipath and geometry effects, *J. geophys. Res.,* **115,** B04403, doi:10.1029/2009JB006543.

King, M.A. & Williams, S.D.P., 2009. Apparent stability of GPS monumentation from short-baseline time series, *J. geophys. Res.,* **114,** B10403, doi:10.1029/2009JB006319.

Meindl, M., 2011. Combined Analysis of Observations from Different Global Navigation Satellite Systems, *Phd dissertation,* Astronomical Institute University of Bern, Switzerland.

Ostini, L., Beutler, G., Dach, R., Hugentobler, U., Ploner, M., Schaer, S. & Urschl, C., 2007. Near-seasonal periods in GNSS station time series, *Geophys. Res. Abstr.,* **9,** 06586.

Penna, N.T., King, M.A. & Stewart, M.P., 2007. GPS height time series: short-period origins of spurious long-period signals, *J. geophys. Res.,* **112,** B02402, doi:10.1029/2005JB004047.

Petit, G. & Luzum, B.e., 2010. *IERS Conventions (2010), (IERS Technical Note ; 36) Frankfurt am Main: Verlag des Bundesamts für Kartographie und Geodäsie, 2010*. 179 pp., ISBN 3-89888-989-6.

Ray, J., Altamimi, Z., Collilieux, X. & Dam, T., 2007. Anomalous harmonics in the spectra of GPS position estimates, *GPS Solut.,* **12**(1), 55–64.

Ray, J., Griffiths, J., Collilieux, X. & Rebischung, P., 2013. Subseasonal GNSS positioning errors, *Geophys. Res. Lett.,* **40**(22), 5854–5860.

Rebischung, P., Ray, J., Benoist, C., Métivier, L. & Altamimi, Z., 2015. *Error analysis of the IGS repro2 station position time series,* Abstract G23B-1065, Presented at AGU, San Francisco, CA, 14–18 December.

Rebischung, P., Altamimi, Z., Ray, J. & Garayt, B., 2016. The IGS contribution to ITRF2014, *J. Geod.,* **90**(7), 611–630.

Rodriguez-Solano, C.J., Hugentobler, U., Steigenberger, P. & Lutz, S., 2011. Impact of Earth radiation pressure on GPS position estimates, *J. Geod.,* **86**(5), 309–317.

Rodriguez-Solano, C.J., Hugentobler, U. & Steigenberger, P., 2012. Adjustable box-wing model for solar radiation pressure impacting GPS satellites, *Adv. Space Res.,* **49**(7), 1113–1128.

Rodriguez-Solano, C.J., Hugentobler, U., Steigenberger, P., Bloßfeld, M. & Fritsche, M., 2014. Reducing the draconitic errors in GNSS geodetic products, *J. Geod.,* **88**(6), 559–574.

Santamaría-Gómez, A. & Mémin, A., 2015. Geodetic secular velocity errors due to interannual surface loading deformation, *Geophys. J. Int.,* **202**(2), 763–767.

Schöne, T., Schön, N. & Thaller, D., 2009. IGS Tide Gauge Benchmark Monitoring Pilot Project (TIGA): scientific benefits, *J. Geod.,* **83,** 249–261.

Sidorov, D. & Teferle, F., 2016. Impact of antenna phase centre calibrations on position time series: preliminary results, *Int. Assoc. Geodesy Symposia,* pp. 117–123.

Steigenberger, P., Lutz, S., Dach, R., Schaer, S. & Jäggi, A., 2014. *CODE repro2 Product Series for the IGS,* Astronomical Institute, University of Bern, URL: http://www.aiub.unibe.ch/download/REPRO_2013.

Teferle, F.N., Bingley, R.M., Dodson, A.H. & Baker, T.F., 2002. Application of the dual-CGPS concept to monitoring vertical land movements at tide gauges, *Phys. Chem. Earth,* **27**(32–34), 1401–1406.

Teferle, F.N., Orliac, E.J. & Bingley, R.M., 2007. An assessment of Bernese GPS software precise point positioning using IGS final products for global site velocities, *GPS Solut.,* **11**(3), 205–213.

Tregoning, P. & Watson, C., 2009. Atmospheric effects and spurious signals in GPS analyses, *J. geophys. Res.,* **114,** B09403, doi:10.1029/2009JB006344.

Wanninger, L. & Wallstab-Freitag, S., 2007. Combined processing of GPS, GLONASS, and SBAS code phase and carrier phase measurements, in *Proc. ION GNSS 2007,* Fort Worth, TX, 2007 September 25–28, pp. 866–875.

Zumberge, J.F., Heflin, M.B., Jefferson, D.C., Watkins, M.M. & Webb, F.H., 1997. Precise point positioning for the efficient and robust analysis of GPS data from large networks, *J. geophys. Res.,* **102**(B3), 5005–5017.